

Wavelet power spectrum analysis of a nonstationary nonlinear time series data

1stManaswita Das
 Department of Mathematics
 Techno India University, West Bengal
 Kolkata, India
bidisha206@gmail.com

2ndMourani Sinha
 Department of Mathematics
 Techno India University, West Bengal
 Kolkata, India
mou510@gmail.com

Abstract—The significant wave height (SWH) data variability is studied for the Bay of Bengal region for the period 1996-2000 using continuous wavelet power spectrum. The averaged SWH time series were normalized by their standard deviation and then decomposed using the Morlet wavelet function. The normalized wavelet power spectrum are generated with the cone of influence, where edge effects become important. The 95% confidence level for the SWH data is shown by the black contours. For a red-noise process the significance levels were computed with a lag-1 coefficient of 0.99. For white-noise process similar contours were generated with a lag-1 coefficient of 0.00 since they are uncorrelated in time. For the year 1996 the red-noise wavelet power spectrum shows two bands of oscillations, one in the 5-20 days period and the other one in the 32-64 days period. Except for the year 2000 the maximum power is concentrated in the June-August months for the 32-64 day period. In spite of the above fact significant region is noted only in the year 1996 for the 32-64 day period. Hence the red-noise wavelet power spectra effectively captures the oscillations in the SWH data which corresponds to seasonal variations.

Keywords—Time series, fourier transform, wavelet power spectrum, significant wave height, Bay of Bengal.

I. INTRODUCTION

A wavelet can be defined as a wave like oscillation that develops from zero amplitude and then reaches a maximum value and then finally decreases back to zero amplitude. A wavelet has an oscillation period, a maximum point and a scale such that it amplifies and declines and are used in various fields like signal analysis, image processing and data compression. In the 1980's wavelet analysis developed in mathematical studies and then applied in geophysics in the next decade. Raw signals may contain information that are easily not available and thus mathematical transformations are used to extract more information. Primarily the signals are time domain ones and thus are functions of time. On plotting these signals one obtains a time and amplitude graph of the given signal. For most of the signal processing studies and applications, such graphs may not represent the signal appropriately. The frequency part of the signal may contain important information which remain hidden. If the Fourier Transform of the signal is performed in the time domain one obtains a frequency and amplitude graph of the given signal.

The Fourier transform acts as a powerful tool to evaluate the frequency content of a given signal. For the Fourier transform if the entire time axis is considered, the information for the rise of a particular frequency is lost. Instead short time Fourier transform can be used which uses a sliding window to find the spectrogram. Although this

gives information of time and frequency both, due to the length of window the resolution of the frequency gets limited. However the problem can be solved using wavelet transform which are based on small wavelets having limited duration.

In 1909, the mathematician Alfrd Haar mentioned wavelet transform for the first time in literature in the form of Haar wavelet. At that time the definition of wavelets were not known and it was geophysicist Jean Morlet in 1981 who gave the idea. The term wavelet was invented in 1984 by Morlet and Alex Grossman. The only known orthogonal wavelet was the Haar wavelet till in 1985, Yves Meyer formed the second orthogonal wavelet known as the Meyer wavelet. Stephane Mallat and Meyer gave the idea of multiresolution in 1988 and Ingrid Daubechies constructed orthogonal wavelet having compact support in the same year. Mallat proposed a fast wavelet transform in 1989 which had applications in the field of signal processing.

The wavelet transform has been used in various studies which includes the El Niño–Southern Oscillation [1, 2] and the turbulent flows [3]. Reference [4] used orthogonal (Haar) and continuous (Morlet) wavelet transform on synthetic and real data. There are studies related to atmospheric cold fronts [5] in which wavelet transform proved to be superior compared to other transform methods. Trends in temperature data from 1659 to 1990 have been studied using wavelet analysis [6]. Reference [7] shows the usefulness of the wavelet transform by studying the dispersion of the Yanai waves. In comparison to Fourier transform, developments due to wavelet transform are discussed in analyzing phase relations, as wind generated wave grows and wave breaks [8]. Reference [9] gives the theoretical aspect of the wavelet analysis while [10] describes the geophysical applications. Reference [11] introduces wavelet analysis comprehensively but avoided the issue of statistical significance.

Spectral analysis is a mechanism that can extract embedded features in a time series. In particular, Fourier analysis has been used extensively by researchers for extracting deterministic structures from time series but is incapable of detecting non stationary features often present in geophysical time series. Using wavelet analysis short term characteristics embedded in time series can be extracted. The wavelet power spectrum being a function of time and period represents the variance or power of a time series. After the pioneering work by [12], wavelet analysis has been widely used to analyze geophysical time series data like the North Atlantic Oscillation indices [13], Arctic Oscillation time series data [14], Pacific Decadal Oscillation time series data [15, 16], El Niño–Southern Oscillation [17], Pacific–North

American pattern, and west Pacific pattern [18]. Wavelet coherence and cross-wavelet analyses [19] have been performed and shown more useful for analyzing geophysical time series data [14, 18, 19, 20]. Irregular waves are often described by a spectrum that indicates the amount of wave energy at different wave frequencies. Significant wave height estimates are having a wide application in coastal and offshore engineering studies. For ocean wave energy studies the spatial variation of the significant wave height data is crucial. Thus, estimation and analysis of significant wave height is important. Reference [21] assess the influence of monsoon variability on the surface waves using continuous wavelet transform. The continuous wavelet power spectra of half-hour significant wave height (SWH) during monsoon in different years present two bands of oscillations: one in the 8–16-day band and the other one in the 4–8-day band.

In the present work continuous wavelet power spectra are generated using six hourly averaged significant wave height time series data over Bay of Bengal (BOB) for the years 1996 to 2000. Significance levels were determined for both white-noise and red-noise processes along with computed lag-1 auto correlations.

II. DATA

ERA-40 analyzed ocean wave dataset of the European Centre for Medium-Range Weather Forecasts (ECMWF) from 1996 to 2000 for the Bay of Bengal (BOB) region (78E to 98E and 25N to 5N) was used to study the significant wave height (SWH) variability. The spatial resolution of the dataset is one degree by one degree and the temporal resolution is six hours. Averaged over the BOB region SWH time series ($N = 1460$) were generated for the years 1996 to 2000 separately for wavelet analysis.

III. METHODOLOGY

A time series can be estimated using wavelet transform which contain for different frequencies nonstationary power (Daubechies 1990). Let there be a time series, x_n , with equal time spacing Δt and $n = 0 \dots N - 1$ and a wavelet function $\psi_0(t)$, that depends on a nondimensional time parameter t . For the function to be a wavelet, it must have zero mean and be localized in time and frequency space [3]. The Morlet wavelet is an example given by $\psi_0(t) = \pi^{-1/4} e^{i\omega_0 t} e^{-t^2/2}$, where ω_0 is the nondimensional frequency. In this case ω_0 is 6 so that the function is a wavelet function [3]. Reference [12] demonstrated the wavelet given below

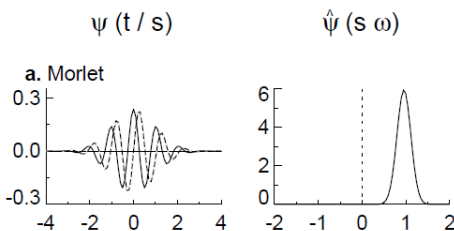


Figure: Morlet wavelet basis

The left hand plot shows the real part given by the solid line and the imaginary part given by the dashed line, of the wavelet in the time domain and the right hand plot gives the

same in the frequency domain. The scale chosen in this case was $s = 10\Delta t$. Generally the term wavelet function is referred to orthogonal or nonorthogonal wavelets while the term wavelet basis is used for orthogonal functions. The use of an orthogonal basis implies the use of the discrete wavelet transform, while a nonorthogonal wavelet function can be used with either the discrete or the continuous wavelet transform [3]. With respect to the work discussed in this paper only the continuous wavelet transform has been utilized.

The continuous wavelet transform of the time series x_n given below, can be stated as the convolution of x_n along with a scaled and translated version of $\psi_0(t)$

$$W_n(s) = \sum_{n'=0}^{N-1} x_{n'} \psi^* \left[\frac{(n' - n)\Delta t}{s} \right]$$

such that the $(*)$ indicates the complex conjugate. The wavelet scale s can be varied and translated along the time index n to show how the amplitude varies with both the scale and the time. Since ψ has been normalized the subscript 0 on ψ in the expression above is not used. From the above expression although the wavelet transform can be calculated, it is much faster when the Fourier space is considered.

The wavelet function $\psi(t)$ being a complex function makes the corresponding wavelet transform $W_n(s)$ also a complex function. Thus the transform can be represented having real and imaginary parts. One can define the wavelet power spectrum as $|W_n(s)|^2$. To compare easily different wavelet power spectra a common normalization is required for the wavelet spectrum. For a white-noise process, the expected value for the wavelet transform is $|W_n(s)|^2 = \sigma^2$, for all n and s , and where σ^2 is the variance.

Figure 2b given in the next section shows the normalized wavelet power spectrum, $|W_n(s)|^2 / \sigma^2$ for the averaged SWH time series. Due to the normalization by $1/\sigma^2$ one obtains a measure of the power with respect to the white noise. In Figure 2b, most of the power is concentrated during June–August in the 32–64 day band.

Although there are several factors which should be considered while performing a wavelet analysis, generally an arbitrary wavelet function, $\psi_0(t)$ is chosen. Some of the factors to be considered are discussed below.

(i) Orthogonal or nonorthogonal:

Wavelet analysis which are orthogonal has at each scale the number of convolutions to be proportional to the wavelet basis width at the same scale. Thus wavelet spectrum with discrete sections of wavelet power is produced and these are useful for representing signals. For time series analysis it is unlucky that a different wavelet spectrum is produced due to the aperiodic shift that occurs in the time series. For a nonorthogonal analysis which are less capable at high scales, the wavelet spectrum is largely correlated at adjacent times. For time series analysis having smooth and continuous variations in wavelet amplitude the nonorthogonal transform is more appropriate.

(ii) Complex or real:

Wavelet functions which are complex gives information regarding amplitude and phase. They are better utilized for functions having oscillatory features. As for the case of a real wavelet function, it gives information for a single component only and are used to isolate peaks or discontinuities.

(iii) Shape:

For time series analysis a wavelet function gives the features contained in the time series. Those time series having jumps or steps a Haar function maybe chosen and those varying smoothly a damped cosine function which is smooth is chosen. For the case of wavelet power spectra, the choice of wavelet function is simpler as it gives similar results. As for complex and nonorthogonal wavelet analysis the Morlet and Paul wavelets are considered. Haar and Daubechies, are orthogonal wavelet functions used widely[4, 22, 23].

For a wavelet function the proportion of the width in real and the Fourier spaces gives the resolution of the function. If the function is narrow in time it will have good time resolution although poor frequency resolution. Reverse occurs to a broad function.

After choosing a wavelet function comes the requirement to define the scales to be used for the wavelet transform. For orthogonal analysis the discrete set of scales described by [3] is used. For the nonorthogonal case an arbitrary set of scales can be used as per requirement. The scales can be written as fractional powers of two as given below

$$s_j = s_0 2^{j\Delta j}, \quad j = 0, 1, \dots, J$$

$$J = \Delta j^{-1} \log_2(N\Delta t / s_0),$$

In the above equations s_0 is the smallest resolvable scale and J is the largest scale. The s_0 should be chosen so that the equivalent Fourier period is approximately $2\Delta t$. The choice of a sufficiently small Δj depends on the width in spectral space of the wavelet function. Considering a Morlet wavelet, a Δj of about 0.5 is the largest value that still gives adequate sampling in scale. For the other wavelet functions, a larger value can be used. With smaller values of Δj finer resolutions are obtained.

In Figure 2b, $N = 1460$, $\Delta t = 1/4$ day, $s_0 = 4\Delta t$, $\Delta j = 0.125$, and $J = 56$, giving a total of 57 scales ranging from 1 day up to 128 days. This value of Δj appears adequate to provide a smooth picture of wavelet power.

The time series used here are having finite length. Thus at the beginning and end of the wavelet power spectrum there are errors. This can be corrected by using zeroes at the end of the time series and after wavelet transform removing them. In the present study the time series is added with zeroes to limit the edge effects and fasten the transform. The cone of influence (COI) is the region within the wavelet spectrum in which edge effects are considered. At each scale the COI is defined as the e-folding time as far as the auto correlation of the wavelet power is considered. The decorrelation time is measured using the size of the COI at each scale, whenever there is a spike in the time series.

To determine significance levels for a wavelet spectra, one first needs to choose an appropriate background spectrum. It is then assumed that different realizations of the geophysical process will be randomly distributed about this

mean or expected background, and the actual spectrum can be compared against this random distribution. For most of the geophysical occurrences, an appropriate background spectrum can be either white noise with a flat Fourier spectrum or red noise having increasing power with decreasing frequency. A previous study by [24] derived the mean and variance of the local wavelet power spectrum. In this work, the theoretical white and red noise wavelet power spectra are derived and compared.

Geophysical time series data can be modeled using either white noise or red noise spectra. A simple model for red noise is the univariate lag-1 autoregressive process given by

$$x_n = \alpha x_{n-1} + w_n$$

such that α is the assumed lag-1 auto correlation, $x_0 = 0$, and w_n is taken from Gaussian white noise.

The discrete Fourier power spectrum of the above after normalizing[25] is

$$P_k = \frac{1 - \alpha^2}{1 + \alpha^2 - 2\alpha \cos(2\pi k / N)}$$

Where $k = 0 \dots N/2$ is the frequency index. The relation can be used to model a red-noise spectrum by selecting an appropriate lag-1 auto correlation. By setting $\alpha = 0$ in the above equation a white-noise spectrum is obtained.

For a white noise spectrum the mean is zero, the variance constant and it is uncorrelated in time. For all frequencies the white noise power spectrum is uniformly spread across. A red noise spectrum is serially correlated in time having zero mean and constant variance. It is such that the correlation coefficient lies between 0 and 1 for the lag-1 auto correlation between two successive time samples. This red-noise was estimated from $(\alpha_1 + \sqrt{\alpha_2}) / 2$, where α_1 and α_2 are the lag-1 and lag-2 auto correlations of the averaged SWH.

The null hypothesis is defined for the wavelet power spectrum as follows:

Let us say that the time series has a mean power spectrum. If the wavelet power spectrum has a peak that is significantly higher than the background spectrum, then for a certain percent confidence the peak is assumed to be a true feature. Significant at the 5% level is equivalent to the 95% confidence level, and implies a test against a certain background level. Again 95% confidence interval refers to the range of confidence about a given value. The 95% confidence level for the SWH data is shown by the black contours. During May-August of the year 1996 there is a continuous significant region in the 32-64 days period (figure 2b). The 95% confidence implies that 5% of the wavelet power should be above this level.

IV. RESULTS AND DISCUSSIONS

SWH data have been downloaded for the BOB region from the ECMWF analyzed ERA-40 global ocean datasets from 1996 to 2000. It has spatial resolution one degree by one degree and temporal resolution six hours. The BOB region extends from 78E to 98E longitude and 25N to 5N latitude. For each year separately averaged SWH time-series were generated where $N = 1460$.

The time-series were standardized by their standard deviation and then decomposed using the Morlet wavelet function. The normalized wavelet power spectrum are generated with the cone of influence, where edge effects become important. Anything below it is taken to be doubtful. The black contour encloses regions of greater than 95% confidence for a red-noise process with a lag-1 coefficient of 0.99. For white-noise process similar contours were generated with a lag-1 coefficient of 0.00 since they are uncorrelated in time.

Fig 1a gives the time-series plot of averaged BOB SWH for the year 1996 with an annual mean SWH of 0.99 m, minimum and maximum wave height of 0.56 m and 2.03 m respectively. The x-axis represents time in days and y-axis SWH in meter. The peaks are observed during the months of June, July and August during the southwest monsoon season when the region is under the influence of strong local winds.

Fig 1b gives a sharp peak of 2.16 m in the month of May for the year 1997. The mean wave height is approximately 1 meter but higher values spread over a longer period, from May to August. Fig 1c represents the year 1998 with mean 0.99 m and maximum value of 1.66 m. High magnitudes prevails from June to September. Fig 1d and fig 1e represents the year 1999 and 2000 with mean wave heights 1.05 m and 1.04 m respectively. Both having a maximum of 1.8 m, with higher waves during the southwest monsoon season. Thus we can say the averaged SWH time-series data show oscillations with periods 30-100 days.

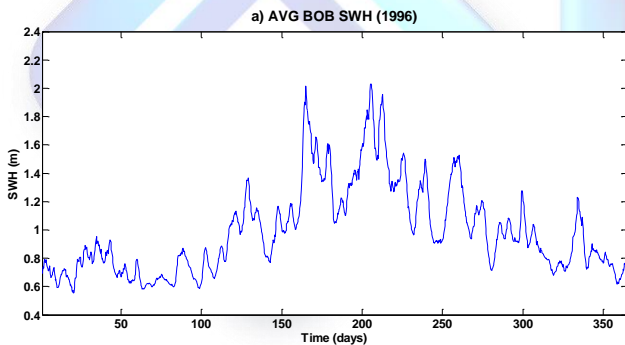


Fig. 1a. Time-series of averaged BOB SWH for 1996

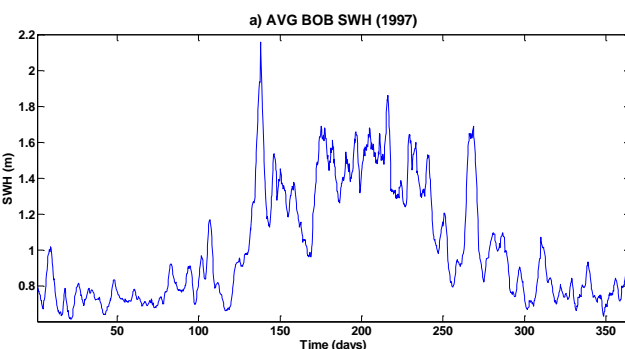


Fig. 1b. Time-series of averaged BOB SWH for 1997

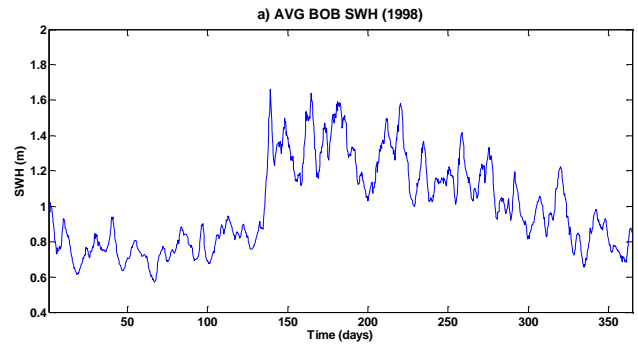


Fig. 1c. Time-series of averaged BOB SWH for 1998

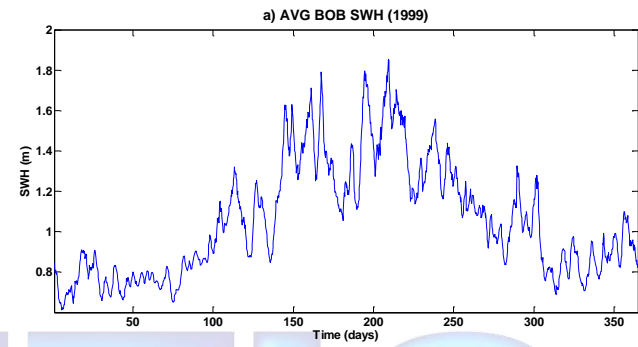


Fig. 1d. Time-series of averaged BOB SWH for 1999

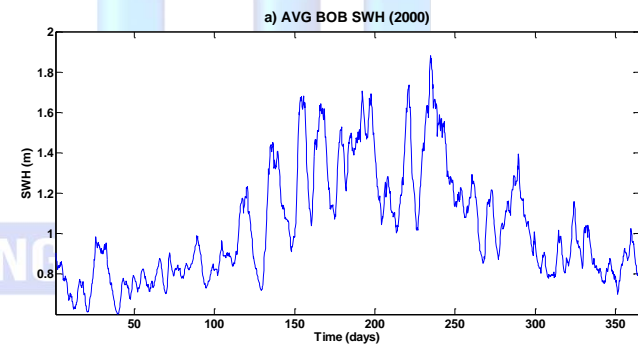


Fig. 1e. Time-series of averaged BOB SWH for 2000

The wavelet transforms identifies the localized intermittent periodicities in a time series which are expanded using the transform into time frequency space. A time series is represented using continuous wavelet transform into a time frequency space such that the oscillations having different periods are observed. The continuous wavelet power spectra of six-hourly SWH in different years are presented below. Fig 2a gives the averaged BOB SWH time-series data for 1996 normalized by standard deviation. The pattern is same as fig 1a but with different y-axis limits.

Fig 2b and fig 2c are the contour plots showing the magnitude of the wavelet power spectrum of the normalized time-series. The x-axis is the wavelet location in time and the y-axis (logarithmic scale) is the wavelet period in days. The black contours are the 95% confidence level with respect to red and white noise. The region below the black curve is the 'cone of influence', where edge effects limit the ability to interpret the results. The colour bar represents the power. For the red-noise process in fig 2b large power occur during the

5-20 day and 32-64 day period. During June, July August there are two oscillations, one in the 5-20 day band and the other one in the 32-64 day band. Among these two bands, the energy in 32-64 day band was continuous and throughout the time-series. For the 5-20 day band there are isolated significant regions only. Fig 2c has a power spectrum for the white-noise process which has black contours spread across denoting no significant regions.

Fig 3a, 3b, 3c gives similar plots for 1997. The red-noise power spectrum (fig 3b) shows two bands of oscillations like 1996 but there is no significant region during July-August. Time-series and contour plots in figures 4, 5 and 6 represents the years 1998, 1999 and 2000. For the year 1998, the wavelet power spectrum (fig 4b) shows a small significant region during June-July at a period of 32 day. From April onwards there are significant regions in the 8-16 day period. The red-noise power spectrum (fig 5b) of 1999 shows continuous large power in the 32-64 day band like 1996 but there is no significant contour at the 95% confidence level. Fig 6b of the year 2000 shows significant regions only at the 8-16 day period. The regions represents the peak of the time series.

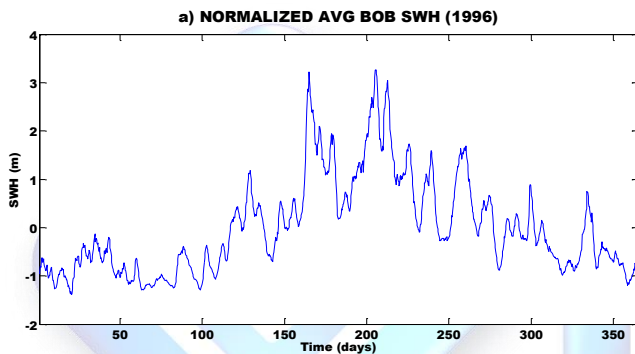


Fig. 2a. Averaged BOB SWH time-series data for 1996 normalized by standard deviation.

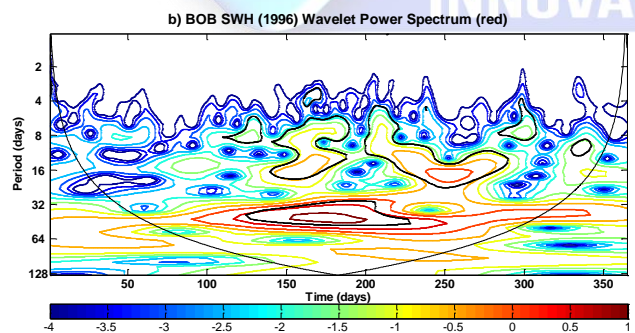


Fig. 2b. The local wavelet power spectrum for 1996 using the Morlet wavelet. The black contours are the 5% significance regions, using a red-noise background spectrum.

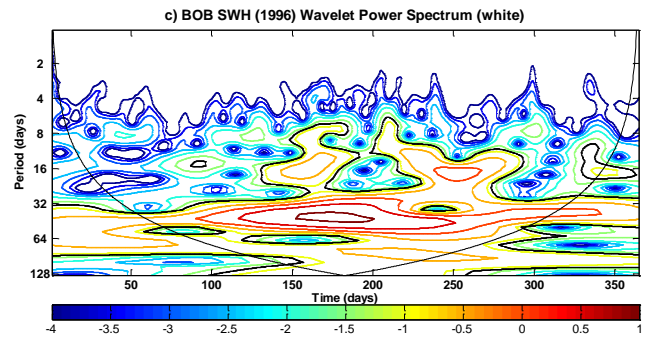


Fig. 2c. Same as figure 2b except for white-noise background spectrum.

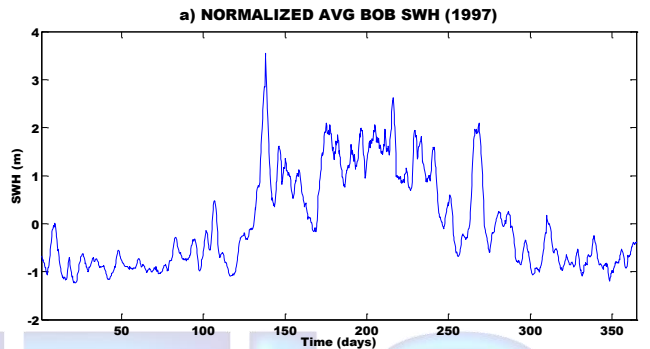


Fig. 3a. Averaged BOB SWH time series data for 1997 normalized by standard deviation

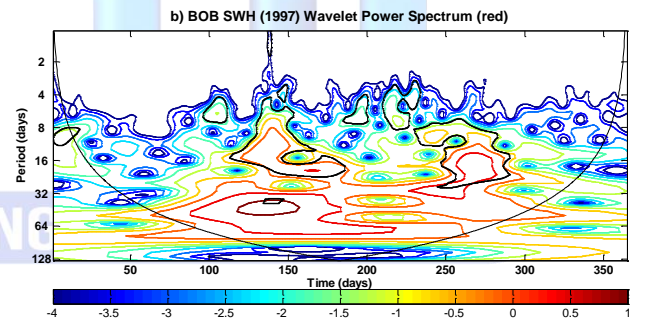


Fig. 3b. The local wavelet power spectrum for 1997 using the Morlet wavelet. The black contours are the 5% significance regions, using a red-noise background spectrum.

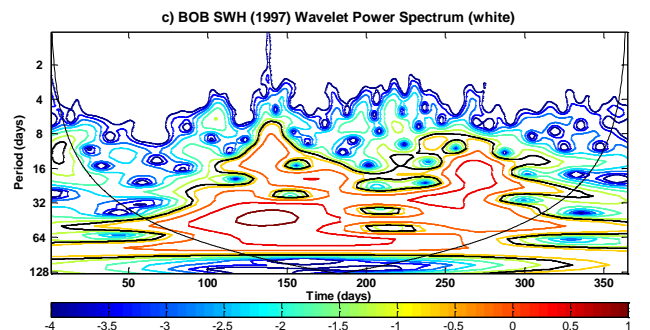


Fig. 3c. Same as figure 2b except for white-noise background spectrum.

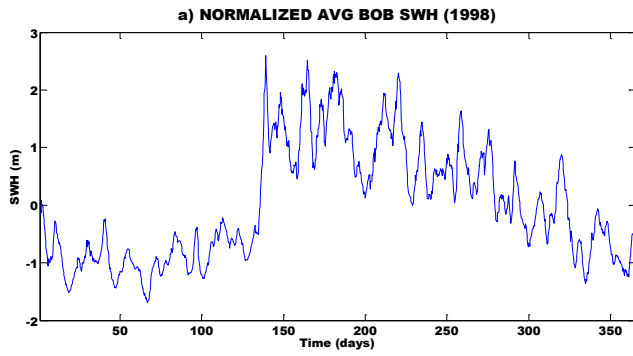


Fig. 4a. Averaged BOB SWH time series data for 1998 normalized by standard deviation

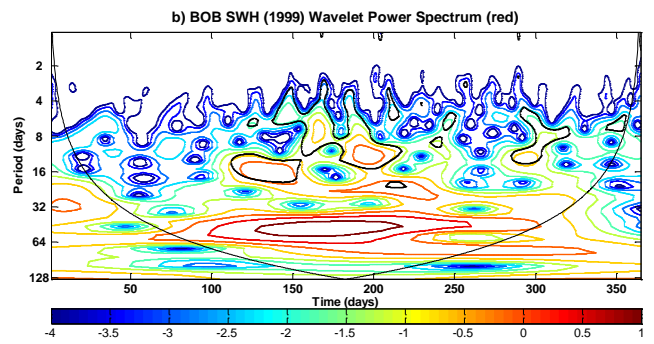


Fig. 5b. The local wavelet power spectrum for 1999 using the Morlet wavelet. The black contours are the 5% significance regions, using a red-noise background spectrum.

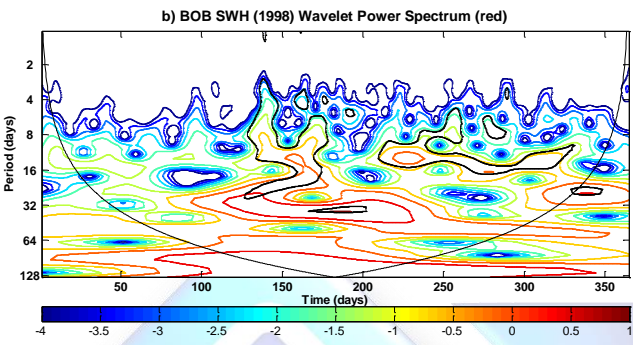


Fig. 4b. The local wavelet power spectrum for 1998 using the Morlet wavelet. The black contours are the 5% significance regions, using a red-noise background spectrum.

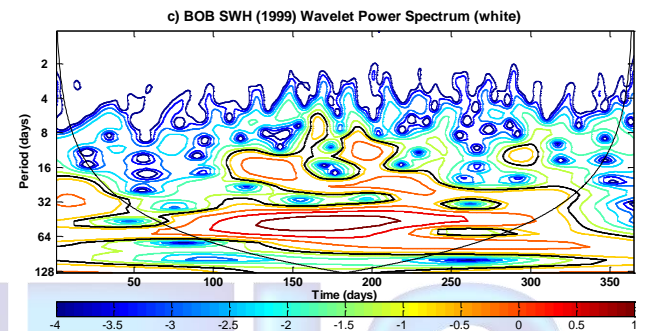


Fig. 5c. Same as figure 2b except for white-noise background spectrum.

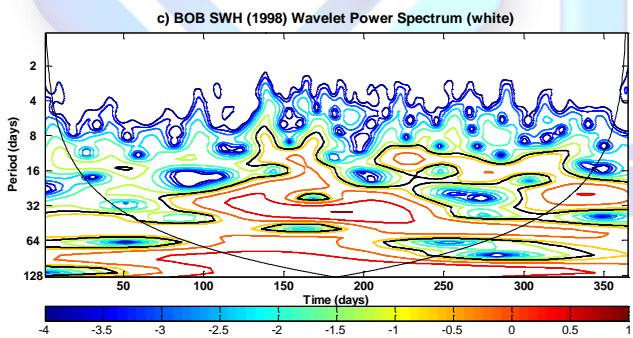


Fig. 4c. Same as figure 2b except for white-noise background spectrum.

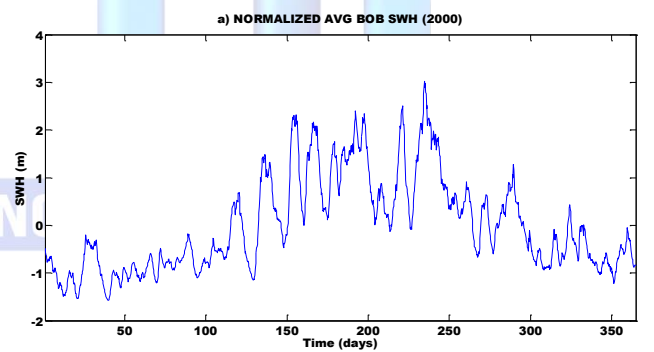


Fig. 6a. Averaged BOB SWH time-series data for 2000 normalized by standard deviation.

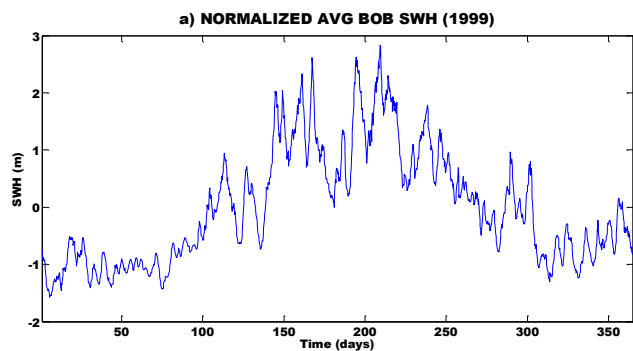


Fig. 5a. Averaged BOB SWH time-series data for 1999 normalized by standard deviation

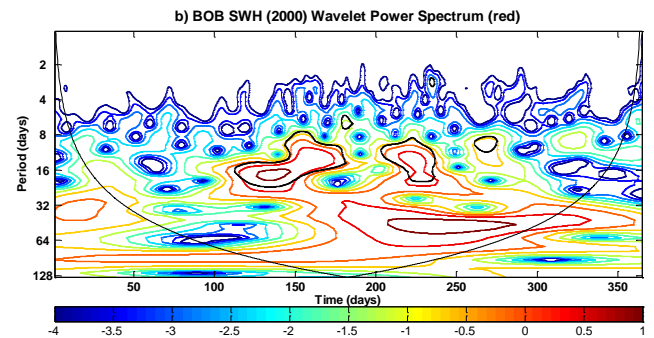


Fig. 6b. The local wavelet power spectrum for 2000 using the Morlet wavelet. The black contours are the 5% significance regions, using a red-noise background spectrum.

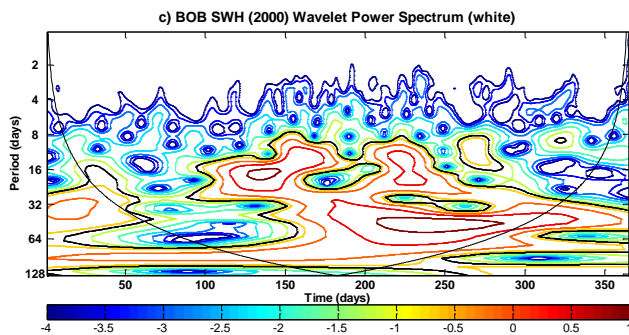


Fig. 6c. Same as figure 2b except for white-noise background spectrum.

V. CONCLUSIONS

For the BOB region averaged SWH time series data are decomposed using the Morlet wavelet function. Continuous wavelet power spectra are generated for the years 1996 to 2000. Confidence levels are determined for both white-noise and red-noise processes along with computed lag-1 auto correlations. During June, July August there are two oscillations, one in the 5-20 day band and the other one in the 32-64 day band for the year 1996. For the red-noise process large power can be seen during the above periods. In 1997 there is no significant region during July-August for the red-noise power spectrum. In 1998 there is an extended region in the 8-16day band from July to October. The year 1999 shows continuous significant region in the 32-64 day period similar to 1996. There is again no significant region during July in the year 2000 like 1997. Thus we can conclude the red-noise wavelet power spectra effectively captures the oscillations in the SWH data which corresponds to seasonal variations.

ACKNOWLEDGMENT

The authors are thankful to European Centre for Medium-Range Weather Forecasts (ECMWF) for the data sets.

REFERENCES

- [1] D. Gu, and S. G. H. Philander, "Secular changes of annual and interannual variability in the Tropics during the past century," *J. Climate*, vol. 8, pp. 864–876, 1995.
- [2] Wang, and Y. Wang, "Temporal structure of the Southern Oscillation as revealed by waveform and wavelet analysis," *J. Climate*, vol. 9, pp. 1586–1598, 1996.
- [3] M. Farge, "Wavelet transforms and their applications to turbulence," *Annu. Rev. Fluid Mech.*, vol. 24, pp. 395–457, 1992.
- [4] H. Weng, and K. M. Lau, "Wavelets, period doubling, and time-frequency localization with application to organization of convection over the tropical western Pacific," *J. Atmos. Sci.*, vol. 51, pp. 2523–2541, 1994.
- [5] N. Gamage, and W. Blumen, "Comparative analysis of low level cold fronts: Wavelet, Fourier, and empirical orthogonal function decompositions," *Mon. Wea. Rev.*, vol. 121, pp. 2867–2878, 1993.
- [6] S. Baliunas, P. Frick, D. Sokoloff, and W. Soon, "Time scales and trends in the central England temperature data (1659–1990): A wavelet analysis," *Geophys. Res. Lett.*, vol. 24, pp. 1351–54, 1997.
- [7] S. D. Meyers, B. G. Kelly, and J. J. O'Brien, "An introduction to wavelet analysis in oceanography and meteorology: With application to the dispersion of Yanai waves," *Mon. Wea. Rev.* vol. 121, pp. 2858–2866, 1993.
- [8] P. C. Liu, "Wavelet spectrum analysis and ocean wind waves," *Wavelets in Geophysics*, E. Foufoula-Georgiou and P. Kumar, Eds., Academic Press, pp. 151–166, 1994.
- [9] I. Daubechies, "The wavelet transform time-frequency localization and signal analysis," *IEEE Trans. Inform. Theory*, vol. 36, pp. 961–1004, 1990.
- [10] E. Foufoula-Georgiou, and P. Kumar, Eds., *Wavelets in Geophysics*, Academic Press, 373 pp, 1995.
- [11] K. M. Lau, and H. Y. Weng, "Climate signal detection using wavelet transform: How to make a time series sing," *Bull. Amer. Meteor. Soc.*, 76, 2391–2402, 1995.
- [12] C. Torrence, and G. P. Compo, "A Practical Guide to Wavelet Analysis," *Bull. Am. Meteorol. Soc.*, vol. 79, pp. 61–78, 1998.
- [13] J. Olsen, J. N. Anderson, and M. F. Knudsen, "Variability of the North Atlantic Oscillation over the past 5,200 years," *Nat. Geosci.*, vol. 5, pp. 808–812, 2012.
- [14] S. Jevrejeva, J. C. Moore, and A. Grinsted, "Influence of the Arctic Oscillation and El Nino-Southern Oscillation (ENSO) on Ice Conditions in the Baltic Sea: The wavelet Approach," *J. Geophys. Res.*, vol. 108, D214677, 2003.
- [15] G. M. MacDonald, and R. A. Case, "Variations in the Pacific Decadal Oscillation over the Past Millennium," *Geophys. Res. Lett.*, vol. 32, L08703, 2005.
- [16] M. Newman, G. P. Compo, and M. A. Alexander, "ENSO-forced variability of the Pacific decadal oscillation," *J. Clim.*, vol. 16, pp. 3853–3857, 2003.
- [17] C. Torrence, and P. J. Webster, "Interdecadal Changes in the ENSO–Monsoon System," *J. Clim.*, vol. 12, pp. 2679–2690, 1999.
- [18] T. Y. Gan, A. K. Gobena, and Q. Wang, "Precipitation of Southwestern Canada: Wavelet, Scaling, Multifractal Analysis, and Teleconnection to Climate Anomalies," *J. Geophys. Res.*, vol. 112, 2007.
- [19] A. Grinsted, J. C. Moore, and S. Jevrejeva, "Application of the CrossWavelet Transform and Wavelet Coherence to Geophysical Time Series," *Nonlinear Proc. Geoph.*, vol. 11, pp. 561–566, 2004.
- [20] Y. J. Lee, and K. M. Lwiza, "Factors Driving Bottom Salinity Variability in the Chesapeake Bay," *Cont. Shelf Res.*, vol. 28, pp. 1352–1362, 2008.
- [21] V. Sanil Kumar, and J. George, "Influence of Indian summer monsoon variability on the surface waves in the coastal regions of eastern Arabian Sea," *Ann. Geophys.*, vol. 34, pp. 871–885, 2016.
- [22] M. Mak, "Orthogonal wavelet analysis: Interannual variability in the sea surface temperature," *Bull. Amer. Meteor. Soc.*, vol. 76, pp. 2179–2186, 1995.
- [23] R. W. Lindsay, D. B. Percival, and D. A. Rothrock, "The discrete wavelet transform and the scale analysis of the surface properties of sea ice," *IEEE Trans. Geosci. Remote Sens.*, vol. 34, pp. 771–787, 1996.